

Supplementary Information

Designing the Next-Generation of High Capacity Battery Electrodes

Hui-Chia Yu¹, Chen Ling¹, Jishnu Bhattacharya¹, John C. Thomas¹, Katsuyo Thornton¹,
Anton Van der Ven^{1,2*}

¹Department of Materials Science and Engineering, University of Michigan, Ann Arbor,
MI 48109, USA

²Materials Department, University of California Santa Barbara, CA. 93106-5050, USA

* avdv@engineering.ucsb.edu

I. First-principles and Monte Carlo calculations

I.A. First-principles calculation of thermodynamic properties

The thermodynamic properties for the Li-Cu-TiS₂ ternary system within the spinel crystal structure of TiS₂ were calculated with well-established statistical mechanical techniques based on the cluster expansion formalism [1,2] as implemented in our CASM (A clusters approach to statistical mechanics) code [3,4]. The approach relies on the construction of an effective Hamiltonian (a cluster expansion) that describes the energy of the crystal as a function of configurational degrees of freedom. The coefficients of the effective Hamiltonian are fit to first-principles total energy calculations obtained within the generalized gradient approximation (GGA) to density functional theory (DFT). Monte Carlo simulations are then applied to calculate finite temperature thermodynamic properties, including relationships between free energies, chemical potentials and concentrations.

To mathematically represent the ternary configurational degrees of freedom associated with all the possible ways of distributing Li, Cu and vacancies over the interstitial sites of spinel TiS₂ (i.e. the 8a and 16c sites within the $Fd\bar{3}m$ space group, with Ti and S occupying the 16d and 32e sites respectively), we assign occupation variables to each interstitial site. First-principles total energy calculations show that Li is stable in both the octahedral and tetrahedral sites of spinel TiS₂, energetically preferring the octahedral sites [5], while Cu only occupies the tetrahedral sites. Hence, the octahedral sites will only have

binary disorder (Li-vacancy) while the tetrahedral sites will have ternary disorder (Cu, Li and vacancies). For each octahedral site, we assign an occupation variable p_i^{Li} that is equal to 1 if site i is occupied by Li and 0 if it is vacant. For each tetrahedral site, we assign two occupation variables, p_j^{Li} and p_j^{Cu} . Just as with the octahedral site, p_j^{Li} for the tetrahedral site is equal to 1 if site j is occupied by Li and 0 otherwise, and p_j^{Cu} is equal to 1 if site j is occupied by Cu and 0 otherwise. Within the cluster expansion formalism, the total energy can then be written as an expansion in terms of products of occupation variables belonging to clusters of sites according to

$$E(\underline{\underline{p}}) = V_o + \sum_{\alpha} V_{\alpha} \cdot \Phi_{\alpha}(\underline{\underline{p}}) \quad (\text{S1})$$

where $\underline{\underline{p}} = \{p_1^{Li}, \dots, p_i^{Li}, \dots, p_{2N}^{Li}, p_1^{Cu}, \dots, p_j^{Cu}, \dots, p_N^{Cu}\}$ is the collection of occupation variables for a spinel crystal structure of TiS_2 having $2N$ octahedral sites and N tetrahedral sites. The polynomial basis functions Φ_{α} are defined as products of occupation variables belonging to a cluster of sites within the crystal according to

$$\Phi_{\alpha} = \prod_{i \in \alpha} p_i^A \quad (\text{S2})$$

where i are tetrahedral or octahedral sites belonging to a cluster α (e.g. a pair cluster, a triplet, a quadruplet etc.), and A refers to either Li or Cu. The coefficients in the above cluster expansion, V_o and V_{α} , are called effective cluster interactions and are to be determined from first principles. While the cluster expansion extends over all clusters of sites and permutations of Li and Cu occupation variables over those sites, in practice, it must be truncated above some maximally sized cluster.

The effective cluster interactions (ECI) are usually fit to reproduce the total energies, calculated from first principles, for a number of different configurations. In this work, DFT calculations were performed with the Vienna *ab initio* simulation package (VASP) [6,7] using the generalized gradient approximation with the projector augmented-wave (PAW) functional [8,9] and a cutoff energy of 400.0 eV for the electron plane wave expansion. All ions and the shape and size of the supercells of different Li-Cu-vacancy configurations within spinel TiS_2 were allowed to relax until the forces on all atoms were less than 0.03

eV/Å. We used the TiS_2 , $\text{Cu}_{0.5}\text{TiS}_2$ and LiTiS_2 as the reference state. The cluster expansion was fit to the formation energies of $\text{Li}_x\text{Cu}_y\text{TiS}_2$ defined as:

$$E_f = E_{t,\text{Li}_x\text{Cu}_y\text{TiS}_2} - xE_{t,\text{LiTiS}_2} - yE_{t,\text{Cu}_{0.5}\text{TiS}_2} - (1-x-y)E_{t,\text{TiS}_2} \quad (\text{S3})$$

where $E_{t,\text{Li}_x\text{Cu}_y\text{TiS}_2}$, E_{t,LiTiS_2} , $E_{t,\text{Cu}_{0.5}\text{TiS}_2}$ and E_{t,TiS_2} are the total energies of $\text{Li}_x\text{Cu}_y\text{TiS}_2$, LiTiS_2 , $\text{Cu}_{0.5}\text{TiS}_2$ and spinel TiS_2 , respectively. A total of 256 Li-Cu-vacancy configurations over spinel TiS_2 were calculated and used in the fit of the ECI of a truncated cluster expansion. The cluster expansion contains 8 Li-Li pairs, 18 Li-Li-Li triplets, and 15 Li-Li-Li-Li quadruplets, 6 Cu-Cu pairs, 3 Cu-Cu-Cu triplets and 1 Cu-Cu-Cu-Cu quadruplet along with 7 Li-Cu pairs and 1 Li-Cu triplet interaction. The ability of the cluster expansion fit to reproduce the original energies is illustrated in Fig. S1. The root mean square error is 3.2 meV per $\text{Li}_x\text{Cu}_y\text{TiS}_2$ formula unit.

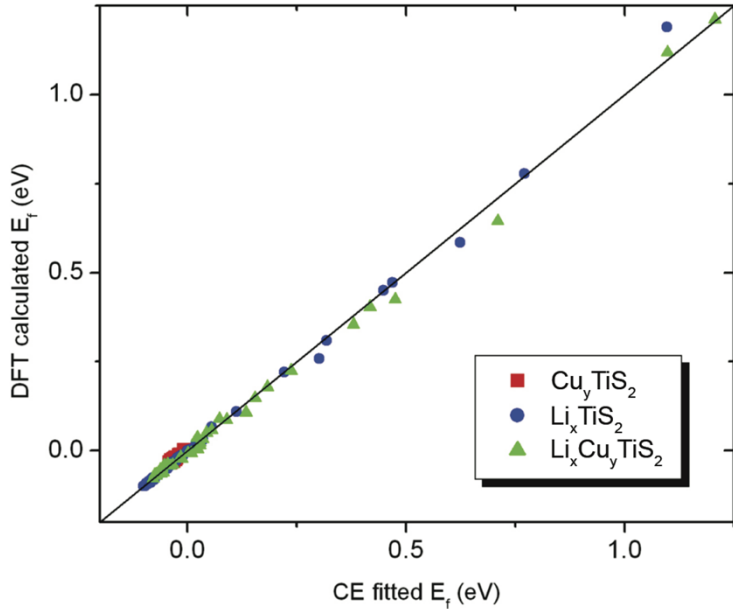


Figure S 1 The cluster expansion fitted formation energies (E_f) versus the formation energies calculated by DFT for the same configuration.

Grand Canonical Monte Carlo simulations were performed in a spinel crystal with periodic boundary conditions containing $12\times 12\times 12$ spinel primitive cells. The average composition of Li and Cu was calculated as a function of chemical potential. The grand

canonical and Gibbs free energies were subsequently obtained through free energy integration in ternary chemical potential space [10] using the energies of TiS_2 , $\text{Cu}_{0.5}\text{TiS}_2$ and LiTiS_2 as the reference states. The ternary phase diagram was then calculated by determining the crossing points of the grand canonical free energies determined from Monte Carlo simulations that traversed from low to high chemical potential and from high to low chemical potential. Hysteresis in Monte Carlo simulations around first-order phase transitions (two-phase regions in the present context) allows us to calculate meta-stable free energies that extend into the two-phase regions to some degree. Crossing points of grand canonical free energies as a function of chemical potentials are equivalent to the common tangent construction applied to the Gibbs free energy. While $\text{Li}_x\text{Cu}_y\text{TiS}_2$ exhibits a variety of stable ordered phases at zero Kelvin, our Monte Carlo simulations indicated that Li and Cu form a disordered solid solution over the interstitial sites of spinel TiS_2 at 300 K. We found no evidence of Li-Cu-vacancy ordering at room temperature as manifested by steps in the chemical potential curves as a function of concentration. We did not explore order-disorder reactions below 300 K.

The free energy obtained from first principles and Monte Carlo simulations is only defined for regions in the $\text{TiS}_2\text{-Cu}_{0.5}\text{TiS}_2\text{-LiTiS}_2$ ternary composition space where the solid solution is stable or metastable. Regions where the curvature of the free energy surface is negative (i.e. the solid solution is unstable) are inaccessible with Monte Carlo simulations. The free energy inside the spinodal was therefore described with a downward parabolic surface for the two-phase region. The free energy within the spinodal was parameterized such that appropriate interfacial energy and interfacial thickness of the phase boundary are determined along with the gradient energy coefficient as $\gamma \sim (2\kappa\sqrt{2h})/3$ and $\xi_l \sim \kappa/\sqrt{2h}$ respectively, where κ is the gradient energy coefficient and h is the barrier height of the free energy function. Here, we set the height of the downward parabolic surface to be 0.09 eV. The selection of this value was motivated by first-principles calculated mixing energies. The Li-octahedra share faces with the Cu-tetrahedra in the spinel host of TiS_2 . Along the $\text{Cu}_{0.5}\text{TiS}_2\text{-LiTiS}_2$ composition line, Li and Cu will by necessity occupy octahedral and tetrahedral sites that share faces, which has a large energy penalty associated with it. For example, the mixing energy for $\text{Li}_2\text{Cu}(\text{TiS}_2)_4$ relative to $\text{Cu}_{0.5}\text{TiS}_2$ and LiTiS_2 whereby Li and Cu are arranged to minimize the number of filled face-sharing Cu tetrahedra and Li octahedra

was calculated to be 0.09 eV per formula unit. Other configurations that increase the number of shared tetrahedron/octahedron faces have higher mixing energies.

Diffusion smoothing of the constructed free energy surface was performed such that its derivatives with respect to concentrations are smooth. Note smoothing was only conducted in the two-phase region while the values of the free energy for compositions where the solid solution is stable remain unaltered from that determined by Monte Carlo. Figure S2 shows the contour plot of the free energy surface obtained by the method mentioned above. Since it is very difficult to interpolate the overall free energy surface in polynomial functions, we instead calculated the chemical potentials using a finite difference scheme from the discrete data points and tabulated the values of individual data points. In the continuum-level simulations, the chemical potentials were linearly interpolated for the compositions between the tabulated data points.

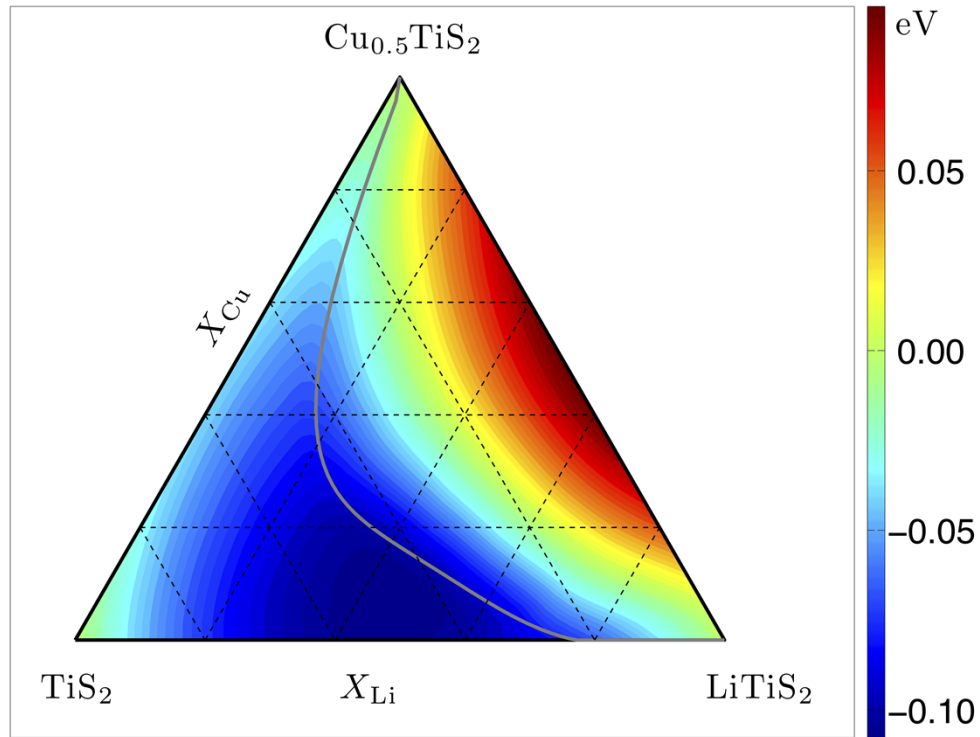


Figure S 2 Color contour of the free energy per interstitial site in spinel $\text{Li}_x\text{Cu}_y\text{TiS}_2$. The area on the left side of the gray line is the solid-solution region calculated from first principles.

I.B. Calculation of diffusion coefficients

Diffusion in electrode particles undergoing displacement reactions is more complex than simple intercalation as two components must diffuse over the interstitial sites of the host. For example Li and Cu diffusion can occur simultaneously in solid solutions of $\text{Li}_x\text{Cu}_y\text{TiS}_2$, sharing interstitial sites of the spinel TiS_2 network. From irreversible thermodynamics, the relevant flux equations take the form

$$J_{Li} = -L_{LiLi}\nabla\mu_{Li} - L_{LiCu}\nabla\mu_{Cu} \quad (\text{S4a})$$

$$J_{Cu} = -L_{CuLi}\nabla\mu_{Li} - L_{CuCu}\nabla\mu_{Cu} \quad (\text{S4b})$$

where L_{ij} are the kinetic transport coefficients and μ_i are chemical potentials. The coefficients L_{ij} can be calculated using Kubo-Green expressions according to [11,12,13]

$$L_{ij} = \frac{\left\langle \left(\sum_{\xi} \Delta \tilde{R}_{\xi}^i(t) \right) \cdot \left(\sum_{\zeta} \Delta R_{\zeta}^j(t) \right) \right\rangle}{(2d)tVk_B T} \quad (\text{S5})$$

where $\Delta \tilde{R}_{\xi}^i(t)$ connects the endpoints of trajectories of atom ξ of type $i = \text{Li}$ or Cu after time t in a crystal of volume V , k_B is Boltzmann's constant, T is the absolute temperature and d is the dimension of the network of interstitial sites. The triangular brackets denote averages in the usual statistical mechanical sense. It is more practical to express the fluxes in terms of gradients of concentration

$$J_{Li} = -D_{LiLi}\nabla C_{Li} - D_{LiCu}\nabla C_{Cu} \quad (\text{S6a})$$

$$J_{Cu} = -D_{CuLi}\nabla C_{Li} - D_{CuCu}\nabla C_{Cu} \quad (\text{S6b})$$

where the matrix of diffusion coefficients D_{ij} is a matrix product of L_{ij} with a matrix of partial derivatives of chemical potentials. As with simple intercalation, all quantities needed to determine the matrix of diffusion coefficients can be calculated by applying grand canonical Monte Carlo simulations (to obtain chemical potentials versus composition) and kinetic Monte Carlo simulations (to evaluate kinetic transport coefficients) to cluster expansions for the configurational energy and migration barriers.

The Kubo-Green expressions can be evaluated explicitly by sampling a large number of representative trajectories within kinetic Monte Carlo simulations. These can be sampled with transition state theory providing stochastic estimates of hop frequencies of atoms to adjacent vacant sites. According to Vineyard [14], these hop frequencies can be estimated as

$$\Gamma = v^* \exp\left(-\frac{\Delta E}{k_B T}\right) \quad (S7)$$

where ΔE is the migration barrier for a hop and v^* is a vibrational prefactor, which in the Harmonic approximation, is equal to the ratio of the product of vibrational frequencies of the solid in the initial state to the product of non-imaginary vibrational frequencies of the solid when the atom is in the activated state.

Due to the large difference between the calculated Li and Cu mobilities in spinel TiS_2 (with typical hop frequencies differing by several orders of magnitude at room temperature) it is not feasible with standard kinetic Monte Carlo simulations to evaluate the full 2×2 matrix of kinetic transport coefficients L_{ij} . Hence in this study we restricted ourselves to predicting diffusion coefficients along the binary $\text{TiS}_2\text{-Cu}_{0.5}\text{TiS}_2$ and $\text{TiS}_2\text{-LiTiS}_2$ axes and then extrapolating these values to the ternary space as described below. For single component interstitial diffusion, the diffusion coefficients appearing in Fick's law can be factored into a product of a thermodynamic factor, Θ , and a kinetic factor, D_J , according to $D = D_J \Theta$ [15] with

$$D_J = \frac{k_B T \Omega}{X} L \quad \text{and} \quad \Theta = \frac{\partial(\mu/k_B T)}{\partial \ln X} \quad (S8)$$

where L is a kinetic transport coefficient obtained using the method as in Eq. (S5), Ω is the volume of the host per interstitial site available, and X is the occupied site fraction of the diffusion species.

The calculation of the Li diffusion coefficient is described in more detail elsewhere [16, 17,18]. All migration barriers were calculated in the cubic unit cell of spinel TiS_2 consisting of 32 sulfur atoms, 16 titanium atoms and variable number of Li or Cu atoms. The nudged elastic band method was used to calculate the migration barrier for Li and Cu hops. A calculation of 30 migration barriers in different Li-vacancy configurations revealed a strong dependence of the barrier on local environment. However, this dependence was only on the immediate local environment, with migration barriers for leaving tetrahedral sites lying in three distinct bands depending on whether the Li atom was hopping into a single vacancy, a divacancy or a triple vacancy [5]. The migration barriers for 8 different Cu-vacancy configurations were also calculated in TiS_2 . The Cu migration barriers were found to be

insensitive (within the numerical error of these calculations, ~25-50 meV) to Cu composition and Cu-vacancy arrangement, having a value around 0.9 eV. Within the kinetic Monte Carlo simulations, the cluster expansion for Li-Cu-vacancy disorder over the interstitial sites of spinel TiS_2 was used to calculate the energies of the end states of the hop. For Li hops, migration barriers were calculated by adding environment dependent barriers to the energy of tetrahedral occupancy [5]. For Cu hops, a constant kinetically resolved migration barrier was added to the average energy of the intial and final states of the hop minus the energy of the initial state of the hop [16]. The vibrational prefactors appearing in Vineyard's expression for atomic hop frequencies were calculated within the local harmonic approximation. Predicted Li and Cu diffusion coefficients along the $\text{TiS}_2\text{-Cu}_{0.5}\text{TiS}_2$ and $\text{TiS}_2\text{-LiTiS}_2$ binary axes are shown in Fig. 2c in the main text.

Calculations of the migration barriers for Li and Cu as a function of the spinel TiS_2 host volume showed that the Li migration barrier increased with decreasing volume while that of Cu decreased with decreasing volume. Since all calculations were performed within the GGA approximation to DFT, which over predicts lattice parameters, we expect that the predicted mobility of Cu is likely underestimated while that of Li is overestimated. For example, we found that the migration barrier of Cu at the equilibrium GGA lattice parameter of TiS_2 (9.83 Å) is almost 100 meV higher than that calculated at the experimental lattice parameter of TiS_2 (9.75 Å). At room temperature, the difference in migration barriers translates into an underprediction of the Cu diffusion coefficient by a factor of 50 (almost 2 orders of magnitude).

We used the calculated diffusion coefficients of the $\text{TiS}_2\text{-Cu}_{0.5}\text{TiS}_2$ and $\text{TiS}_2\text{-LiTiS}_2$ binaries to estimate the diagonal L coefficients for the ternary system. The diagonal L_{ii} coefficients scale directly with the concentration of the diffusing specie i . Furthermore, if the interstitial sites form a lattice and the interstitial atoms behave as an ideal solution, the kinetic transport coefficients will also scale with the concentration of vacancies [19]. For Li and Cu diffusion in spinel TiS_2 , we can therefore to first order write the diagonal transport coefficients for ternary compositions as

$$L_{\text{LiLi}} = X_{\text{Li}} \cdot (1 - X_{\text{Li}}) \cdot (1 - 2X_{\text{Cu}}) \cdot \Lambda_{\text{Li}} \quad (\text{S9a})$$

$$L_{\text{CuCu}} = X_{\text{Cu}} \cdot (1 - X_{\text{Li}}) \cdot (1 - 2X_{\text{Cu}}) \cdot \Lambda_{\text{Cu}}. \quad (\text{S9b})$$

Since the Li and Cu atoms do not occupy the same sublattice, the kinetic coefficients scale with the vacancy concentration on each sublattice. For example, Li hops require the end state of the hop on the octahedral site to be vacant. However, since Li must hop through a tetrahedral site, the intermediate tetrahedral site must also be vacant. Hence, L_{LiLi} should scale with the product of the vacancy concentration on the tetrahedral sublattice, $1-2X_{Cu}$, and the vacancy concentration on the octahedral sublattice, $1-X_{Li}$. In the above expressions, Λ_{Li} and Λ_{Cu} will also depend on the overall concentration, X_{Li} and X_{Cu} , if the migration barriers for the hops depend on concentration and if hop frequencies depend on long and short-range order among the interstitial diffusers (e.g. the divacancy and triple-vacancy hop mechanisms for Li in spinel Li_xTiS_2). In extrapolating our binary diffusion coefficients to the ternary system, we fit Λ_{Li} and Λ_{Cu} such that the diagonal kinetic transport coefficients reproduce the binary kinetic transport coefficients. The mobilities, Λ_i , are related to the self-diffusion coefficients calculated from first principles and kinetic Monte Carlo simulations according to

$$\Lambda_{Li} = \frac{D_J^{Li}}{(1-X_{Li})k_B T \Omega} \quad \text{and} \quad \Lambda_{Cu} = \frac{D_J^{Cu}}{(1-2X_{Cu})k_B T \Omega} \quad (\text{S10})$$

where D_J^{Li} and D_J^{Cu} are the binary self-diffusion coefficients of Li and Cu in TiS_2 crystal, respectively. Note that we have neglected the off-diagonal terms in the Onsager transport coefficients in Eq. (S4), and similarly those in the boundary conditions (insertion/extraction fluxes). While it is a reasonable approximation for most materials, there could be examples, where such approximations are not valid and our general conclusion may not hold.

Substituting Eq. (S10) into Eq. (S9), we obtain

$$L_{LiLi} = [X_{Li} \cdot (1-2X_{Cu}) + \varepsilon_a] \cdot \frac{D_J^{Li}}{k_B T \Omega} \quad (\text{S11a})$$

$$L_{CuCu} = [X_{Cu} \cdot (1-X_{Li}) + \varepsilon_b] \cdot \frac{D_J^{Cu}}{k_B T \Omega} \quad (\text{S11b})$$

where ε_a and ε_b are small values taken to avoid a complete stall in diffusion in the simulations. Here, we choose 0.00025 and 0.000125 for ε_a and ε_b , respectively. They are 0.1% of the maximum values of $X_{Li} \cdot (1-2X_{Cu})$ and $X_{Cu} \cdot (1-X_{Li})$.

As a measure of the asymmetry in Li and Cu mobilities, we defined a parameter, δ , to be $\delta = \bar{D}_{Li} / \bar{D}_{Cu}$, where \bar{D}_{Li} and \bar{D}_{Cu} are the average value of the diffusion coefficients, respectively, over the single-component axes in the composition space; i.e., $\bar{D}_{Li} = \int_0^1 D_{Li}(X_{Li}) dX_{Li} / \int_0^1 dX_{Li}$ and $\bar{D}_{Cu}^{0.5} = \int_0^{0.5} D_{Cu}(X_{Cu}) dX_{Cu} / \int_0^{0.5} dX_{Cu}$. When the value of δ is unity, the mobilities are equal on average, while δ greater than one indicates Li is more mobile than Cu on average. A similar parameter averaging the transport coefficient can be obtained by $\delta_L = \bar{L}_{LiLi} / \bar{L}_{CuCu}$, where the average values of transport coefficients are taken over the ternary composition space as

$$\bar{L}_{LiLi} = \int_0^1 \int_0^{(1-X_{Li})/2} L_{LiLi}(X_{Li}, X_{Cu}) dX_{Cu} dX_{Li} / \int_0^1 \int_0^{(1-X_{Li})/2} dX_{Cu} dX_{Li} \text{ and}$$

$$\bar{L}_{CuCu} = \int_0^1 \int_0^{(1-X_{Li})/2} L_{CuCu}(X_{Li}, X_{Cu}) dX_{Cu} dX_{Li} / \int_0^1 \int_0^{(1-X_{Li})/2} dX_{Cu} dX_{Li}. \text{ In this presented work, the values of } \delta_L \text{ scales with } \delta \text{ by } \delta_L = 0.8749\delta.$$

II. Phase field approach

II.A. Cahn-Hilliard equation

In a phase field model, the chemical potential for transport is given by

$$\mu = \frac{\partial f}{\partial C} - \kappa \nabla^2 C \quad (\text{S12})$$

where f is the bulk free energy (described below), C is the order parameter, and κ is the gradient energy coefficient. For a conserved order parameter (e.g., concentration), the flux is given by $J = -L \nabla \mu$, where L is the transport mobility, and the gradient of the chemical potential provides the driving force. The concentration evolution is governed by mass conservation:

$$\frac{\partial C}{\partial t} = \nabla \cdot L \nabla \left[\frac{\partial f}{\partial C} - \kappa \nabla^2 C \right]. \quad (\text{S13})$$

This equation is known as the Cahn-Hilliard equation. When f has two minima, as in a double-well function, the system tends to separate into two phases (or stay in a two-phase coexistence mixture). This is the case when the composition resides in the two-phase region in the ternary phase diagram shown in the main text. The second term in the chemical

potential panelizes a steep variation of the composition in the interfacial region, and, along with the excess bulk free energy, contributes to the interfacial energy. On the other hand, when f has a single minimum, the system tends to form a single-phase solid solution. This is the case when the composition is in the solid solution region in the ternary phase diagram.

II.B. Smoothed boundary method

To account for the particle geometry in the simulations, we employed the smoothed boundary method [20,21] with a continuous domain parameter, ψ . The region within the particle where Li and Cu transport occurs is defined by volume where $\psi=1$, while the outside of the particle is defined by $\psi=0$. Therefore, the particle surface where Li and Cu are inserted/extracted is automatically defined by the narrow transitioning region where $0 < \psi < 1$. The Cahn-Hilliard equations for Li and Cu are then reformulated [21] into

$$\frac{\partial C_{Li}}{\partial t} = \frac{1}{\psi} \nabla \cdot (\psi L_{LiLi} \nabla \mu_{Li}) - \frac{|\nabla \psi|}{\psi} J_{Li}|_s \quad (\text{S14a})$$

$$\frac{\partial C_{Cu}}{\partial t} = \frac{1}{\psi} \nabla \cdot (\psi L_{CuCu} \nabla \mu_{Cu}) - \frac{|\nabla \psi|}{\psi} J_{Cu}|_s \quad (\text{S14b})$$

where $J_{Li}|_s$ and $J_{Cu}|_s$ are the insertion/extraction fluxes at the particle surface for Li and Cu, respectively, and their expressions are given in the main text.

II.C. Simulation setup

The concentration evolution equations were nondimensionalized by using the length scale l , the reference mobility L_0 , and time scale $\tau = l^2/L_0$. A standard second-order central difference scheme in space and Euler explicit scheme in time were employed to implement the 2D continuum-level simulations. The 2D computational domain contains 176×128 Cartesian grid points, which corresponds to an area of $1.76 \times 1.28 \mu\text{m}^2$. Particle geometry was defined by a continuous domain parameter, ψ , where $\psi=1$ for the interior of the particle and $\psi=0$ for the exterior. The long and short axes of the particle are roughly 150 and 105 grid spacings, respectively. The domain parameter takes the form of

$$\psi = \frac{1}{2} \left[\tanh\left(\frac{\varphi}{\zeta}\right) + 1 \right] \quad (\text{S15})$$

where φ is the dimensionless distance to the particle surface and ζ is used to control the interfacial thickness. By setting $\zeta = 0.5$, the interfacial thickness is roughly 2.2 grid spacings [21], when it is defined by $0.015 < \psi < 0.985$ (approximately 1 grid point when defined by $0.1 < \psi < 0.9$). See Fig. S3 for the particle geometry. The parameters used in the simulations are provided in Table S1.

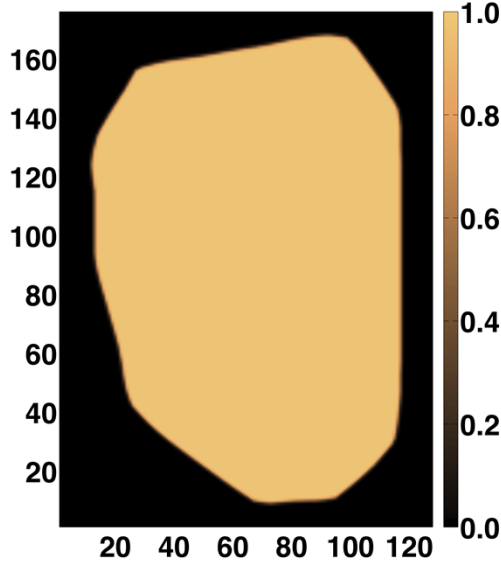


Figure S 3 Continuous domain parameter profile that defines the particle geometry, where the domain parameter value equal to 1 indicates the interior of the particle, the value equal to 0 for the exterior, and the values between 0 and 1 for the particle surface.

III. Additional figures of morphological evolution during discharging

In Fig. S4, we present the snapshots of the morphological evolutions during discharging with $\delta = 100$ and 10000 in addition to that shown in the main text for discharging with $\delta = 1$. The evolutions proceed in a two-phase reaction dynamics where Li-rich regions grow at the expense of Cu-rich regions. A distinguishable difference between the two sets of results can be noted such that the Li-rich regions nucleate in many small particles in the area near the particle surface in the case with $\delta = 100$, whereas the Li-rich regions nucleate in segments of a thin shell in the case with $\delta = 10000$. This morphological difference in the early stage can be attributed to the effect of Cu mobility. When Cu mobility is larger, a deeper penetration

length for Cu is reached, resulting in spherical initial Li-rich phases. In contrast, plate-like initial Li-rich phases form when Cu mobility is small. The Li-rich regions continuously grow and eventually form a complete shell of the particle. Once the shells are completed. The following morphological evolutions for both the two cases are very similar; i.e., a shrinking-core phase boundary motion until the entire particles are lithiated. Although with a discernible difference in the nucleation and early stages of the morphological evolutions, the kinetic reaction paths of discharge for both the two cases, as well as the case with $\delta = 1$, all follow the same edge ($\text{Cu}_{0.5}\text{TiS}_2$ - LiTiS_2) in Fig. 6A in the main text, showing the same two-phase transition from Cu-rich $\text{Cu}_{0.5}\text{TiS}_2$ to Li-rich LiTiS_2 . This is because Li can only enter the crystal when Cu is extruded despite Cu mobility and the corresponding morphology. The simulations clearly demonstrate that the reaction path of discharge is independent of mobility asymmetry between Li and Cu in this displacement reaction.

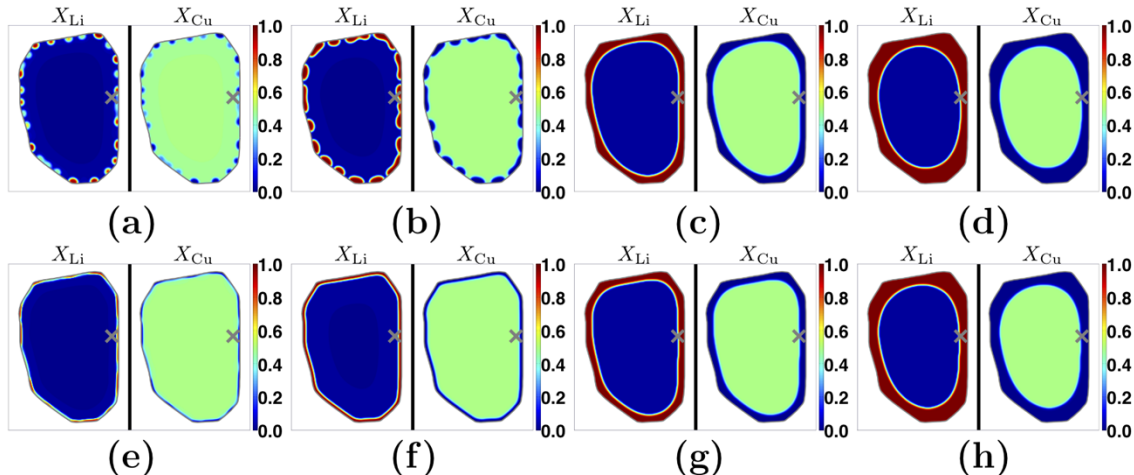


Figure S 4 Snapshots of evolution of Li and Cu in the $\text{Li}_x\text{Cu}_y\text{TiS}_2$ particle during discharge process for (a)-(d) $\delta = 100$ and (e)-(h) $\delta = 10000$. The left and right images in each subfigure are Li and Cu mole fraction profiles, respectively, in the same particle at the same time. The average compositions of the entire particle in (a)-(d) and (e)-(h) are $(\bar{X}_{\text{Li}}, \bar{X}_{\text{Cu}}) = (0.0625, 0.469), (0.125, 0.438), (0.25, 0.375)$, and $(0.375, 0.3125)$, respectively.

Table S 1 The physical parameters used in the continuous simulations.

Grid spacing (l)	10^{-6} cm
Reference mobility (L_0)	1×10^{-9} s $^{-1}$ cm $^{-1}$ eV $^{-1}$
Reaction constant for Li (K_{Li})	2×10^{-3} s $^{-1}$ cm $^{-2}$ eV $^{-1}$
Reaction constant for Cu (K_{Cu})	2×10^{-3} s $^{-1}$ cm $^{-2}$ eV $^{-1}$
Gradient coefficient for Li (κ_{Li})	(eV) $^{1/2} \times l$
Gradient coefficient for Cu (κ_{Cu})	(eV) $^{1/2} \times 2l$
Applied voltage for discharge (Φ)	1.0 V
Applied voltage for charge (Φ)	2.4 V

-
- 1 J. M. Sanchez, F. Ducastelle, D. Gratias, *Physica A*, 128, 334-350 (1984).
- 2 D. de Fontaine, *Solid State Physics*, 47, 33-176 (1994).
- 3 A. Van der Ven, J. C. Thomas, Qingchuan Xu, B. Swoboda, D. Morgan, *Physical Review B* 78, 104306 (2008).
- 4 A. Van der Ven, J. C. Thomas, Q. Xu, J. Bhattacharya, *Mathematics and Computers in Simulation*, 80(7) 1393-1410 (2010).
- 5 J. Bhattacharya, A. Van der Ven, *Physical Review B*, 83, 144302 (2011).
- 6 G. Kresse, J. Furthmuller, *Comput. Mater. Sci.*, 6, 15 (1996).
- 7 G. Kresse, J. Furthmuller, *Phys. Rev. B*, 54, 11169 (1996).
- 8 P. E. Blochl, *Phys. Rev. B*, 50, 17953, (1994).
- 9 G. Kresse, J. Joubert, *Phys. Rev. B*, 59, 1758 (1999).
- 10 Q. Xu, A. Van der Ven, *Intermetallics*, 17 (5), 319-329 (2009).
- 11 A. R. Allnatt, A. B. Lidiard “Atomic transport in solids” Cambridge, Cambridge University Press; (1993).
- 12 R. Zwanzig, *J. Chem. Phys.* 40(9), 2527 (1964).
- 13 A. Van der Ven, H. C. Yu, G. Ceder, K. Thornton, *Progress in Materials Science*, 55 (2), 61-105 (2010).
- 14 G. H. Vineyard, *J. Physics and Chemistry of Solids* 3, 121, (1957).
- 15 R. Gomer, *Reports on progress in physics* 53(7), 917-1002, (1990).
- 16 A. Van der Ven, G. Ceder, M. Asta, P. D. Tepesch, *Physical Review B* 64, 184307, (2001).
- 17 A. Van der Ven, J. C. Thomas, Qingchuan Xu, B. Swoboda, D. Morgan, *Physical Review B*, 78, 104306 (2008)
- 18 A. Van der Ven, J. Bhattacharya, A. A. Belak, *Acc. Chem. Res.* (2012), DOI: 10.1021/ar200329r.
- 19 R. Kutner, *Phys. Lett.* 81A, 239, (1981)
- 20 A. Bueno-Orovio, V. M Peres-Garcia, *Num. Meth. P. D. E.*, 28(3), 886, (2006).
- 21 H.-C. Yu, H.-Y. Chen and K. Thornton, *Model. Simul. Mater. Sci. Eng.* 20(7), 075008, (2012)